Fiber orientation and crimp level might control the auxetic effect of biological tissues

Chenghe Piao, Simon Le Floc'h, Patrick Cañadas, Christiane Wagner-Kocher, Pascale Royer

Fiber orientation and crimp level might control the auxetic effect of biological tissues

C. Piao[1], S. Le Floc'h[1], P. Cañadas[1], C. Wagner-Kocher[1,2], P. Royer[1]

[1]LMGC, Univ. Montpellier, CNRS, Montpellier, France

[2]LPMT, UHA, Mulhouse, France

Abstract

We propose an analytical micromechanical model for studying the lamellar-composite-like structure of fibrous soft tissue. The tissue under consideration is made up of several lamellae, and is designed to resemble the annulus fibrosus (AF) tissue or media layer of arterial tissue, for example. The collagen fibers are arranged in parallel in each lamella and the fiber orientation differs from one lamella to its neighbors. The parallel fibers in each lamella of AF tissue, for example, have been observed to have a crimped microstructure. The proposed model incorporates this quality, considering fiber waviness as a sinusoidal shape and taking into account the fiber dispersion in different layers, where both fiber and matrix are considered as solid phases. We find that collagen-fiber waviness and layer orientation have a significant influence on Poisson's ratio. The effective Poisson's ratio predicted by the proposed model demonstrates that the crimped collagen fiber microstructure might weaken the auxetic effect of fibrous soft tissue, which might explain why, as the literature suggests, the auxetic behavior is more difficult to observe than large Poisson's ratios. As opposed to the many studies that use the well-known hyperelastic fiber-based constitutive model, in which out-of-plane expansion is often observed, the present work explains the auxetic response found in modeling and in experimental data from the perspective of collagen fiber microstructure.

Keywords— Auxetic behavior, Biocomposite, Micromechanics, Constitutive relation, Crimped fibers, Negative Poisson's ratio, Collagen fiber, Fibrous soft tissues, Annulus fibrosus, Arterial tissue

1 Introduction

Fibrous soft tissue composed of several families of collagen fibers is found, for example, in annulus fibrosus (AF) and the media layer of arterial tissues. AF tissue is one of the components that make up the intervertebral discs, which support the movements of the spine. The arteries are vessels that transport blood from the heart to the other tissues and organs of the body. Arteries can be distinguished by their layers: intima, media, and adventitia.

AF and arterial tissues are usually considered as orthotropic materials. Although the linear and nonlinear elastic properties of these tissues are well-established in the literature, the link between their macroscopic behavior and microscopic structure remains only partially understood. The Poisson's ratios of these soft tissues have motivated studies of their internal microstructures; more specifically the collagen fiber structure and arrangement. In recent years,

the auxetic behavior of AF and arterial tissues have received increased attention [1][2]. Some materials or structures exhibit negative Poisson's ratios, and can therefore be described as having an auxetic property, showing unusual and counterintuitive mechanical behavior; when stretched (respectively, compressed), these materials become thicker (respectively, thinner) in the direction perpendicular to that of the load.

Most of the tensile experiments reported in the literature for AF are uniaxial tests [3][4][5] [6][7][8][9], although biaxial tensile tests have also been performed [10][11]. The measurements of the Poisson's ratio for AF reveal a large range of values, from -0.57 [12] to 2.32 [13]. The difference in experimental results could be due to many factors, such as differences in: the types of AF tissue analyzed, the subsections of AF tissue analyzed (inner or outer AF) [3], extension conditions, test specimen status (degenerated or non-degenerated AF), strain-measurement techniques, specimen-storage-solution osmolarity, and so on. Guerin and Elliott [4] and O'Connell et al.[6] found that AF degeneration influences the results of Poisson's ratio measurements. Moreover, Wagner and Lotz [13] showed that the loading type, that is, tension or compression, has an effect on Poisson's ratio results. Furthermore, Derrouiche et al. [12] presented results showing that the different saline concentrations and strain rates used in extension tests also affect such measurements. Although the range of reported Poisson's ratio results is considerable, the orthotropic features of AF along the longitudinal, circumferential, and radial directions are consistently observed. Comparison of the experimental results in the literature reveals that, when loading AF tissue in the the circumferential direction, the Poisson's ratio that characterizes the strain in the radial direction is usually much lower than the Poisson's ratio that characterizes the strain in the longitudinal direction [3][13][8][12]. Even negative $\nu_{\theta r}$ values (auxetic behavior) were recently reported by Baldit et al. [8], Derrouiche et al. [12], and Dusfour et al. [9]. In other words, with extension of AF tissue in the circumferential direction, it is observed to expand in the radial direction in some cases.

In order to predict the mechanical behavior of AF using mechanical modeling, Elliott and Setton [3] implemented a linear anisotropic material model to determine a complete set of model properties under idealized kinematic states. According to the model predictions presented by these authors, interactions between fiber populations in the multilamella AF contribute significantly to the mechanical behavior of the material, suggesting that a model for AF made up of physically isolated concentric lamellae may not be appropriate. Derrouiche et al. [12] presented a chemo-mechanical approach to studying the intrinsic osmo-inelastic response of AF tissue in relation to the microstructure of the layered and reinforced soft tissue, the biochemical environment, and the mechanical loading conditions. This chemo-mechanical approach successfully captured the variations in osmolarity, strain rate, and auxeticity. Kandil et al. [14] proposed a chemo-viscoelastic model as part of a microstructure-based approach to predicting the regional dependency of the annulus response, in which the auxetic behavior is identified in the plane of the lamellae. Dusfour et al. [9] found an auxetic response by applying the HGO model ([15]), but found poor agreement between model and experimental results. Furthermore, AF is widely modeled as a fiber-induced anisotropic hyperelastic material [6][16][17][18]. These models describe the fibers and the matrix using the principle invariants of the Green deformation tensor and structural tensors representing the collagen fiber populations[11].

Several studies have reported measurements of the Poisson's ratio of arteries [19][20][21][22] [23][24][25][26] [27][28][29][30][31]. In most studies, arteries are stretched in an in vitro environment, except for those of Patel et al. [19] and Hasegawa et al. [23], who evaluated the Poisson's ratio of dog and human arteries, respectively, in vivo. However, the Poisson's ratios of arteries reported so far are inconsistent, and both large ($\nu > 1.0$) and negative ($\nu < 0.0$) values have been measured [27], while arteries have been widely observed to be orthotropic along the longitudinal, circumferential, and radial directions. The causes for these significant discrepancies in experimental results could be due to many factors, such as the different types of artery tissue studied [23], the different layers (media or intact vessel) studied, or differences in extension conditions,

strain measurement techniques, test specimen conditions (fresh, or frozen and thawed), and so on. As arterial tissue can be divided into three main types (intima, media, and adventitia), rather than studying the intact arterial wall, more recently the media and adventitia layers were isolated and studied separately [26][27][29][30][31]. Comparing the experimental extension conditions in the literature, the strain velocity, loading pressure, and the maximum stretch strain might also affect the measured values [19][22][20][28][30]. Santamaría et al. [30] and Skacel and Bursa[31] noted that using frozen and thawed artery specimens leads to different experimental results compared to using fresh tissue. Indeed, Santamaría et al. [30] note that frozen and thawed tissues may have nonphysiological hydraulic permeability properties, and that freezing and thawing may cause the destruction of cell membranes. Moreover, several individual negative out-of-plane Poisson's ratios were measured with frozen and thawed test specimens among the 12 specimens used in experiments [29][31] but no negative Poisson's ratio was found in tests with fresh specimens[31]. Negative Poisson's ratios were measured by Timmins et al. [26], Lillie et al. [25], Skacel and Bursa [29], and Santamaría et al. [30] in arterial tissues, and Skacel and Bursa [31] reject their previous experimental observations. In addition, auxetic behaviors have been reported for tendon tissues [32][33][34], skin tissue [35][36], tibia bone [37], axoloti embryonic epithelia [38], and for the bovine cornea [39].

Timmins et al. [26] proposed that the auxetic response could be due to the variable and inhomogeneous alignment of elastin and collagen fibers in the arterial wall. Such lateral expansion was predicted based on a nonlinear hyperelastic anisotropic model of arterial wall with two families of perfectly aligned collagen fibers [15], (known as the HGO model), as presented by Gasser et al. [40], who further proposed a GOH model with dispersed fiber orientations. Skacel and Bursa [29] reported a negative Poisson's ratio exhibited by a GOH model and provided a comprehensive analysis of the auxetic response with distributed fiber orientations. Nolan et al. [41] also identified auxetic behavior with a compressible form of the HGO model called HGO-C, analyzing the predicted lateral stresses induced during uniaxial stretching, and proposed a modified anisotropic (MA) model to avoid them. Similarly, Latorre et al. [42] noticed an unrealistic transversal deformation response predicted by the HGO and GOH models, and proposed their what-you-prescribe-is-what-you-get (WYPIWYG) model as a solution. Volokh [43] applied the HGO model to study auxetic behavior based on the angular integration (AI) approach. Fereidoonnezhad et al. [2] consider that auxetic behavior is primarily influenced by the ratio of fiber-to-matrix stiffness and is accentuated by strain-stiffening fibers in a constant stiffness matrix. These authors propose a bilinear strain-stiffening fiber and matrix model (BLFM), which allows close control of the fiber–matrix stiffness ratio to eliminate auxetic behavior.

The AF and media layer of arterial tissue consist of several families of collagen fibers, in which the collagen fibers are observed to have a crimped microstructure. With our study, we aim to investigate the microstructure function mechanism in fibrous soft tissue such as AF and arterial media so as to understand how material microstructure parameter characteristics might regulate the macroscopic effective Poisson's ratio. We adopt the method of Xiao et al. [44] to find the effective stiffness matrix of composite reinforced with fibers of a particular sinusoidal waviness. Then, our proposed model takes into account the fiber dispersion in different families of collagen fibers and considers fiber waviness as a sinusoidal shape. The layout of the present paper is as follows: section 2 presents the micromechanical model we use to predict the constitutive relations of a tissue-like biocomposite and section 3 summarizes the mechanical parameters of the tissue found in the literature and provides the material parameters used to study its mechanical behavior. In Section 4, we present our theoretical calculation results and compare them with different studied cases of physiological ranges found in real tissues. This is followed by a discussion of the implications and limitations of our micromechanical model and our conclusions in section 5.

2 Micromechanical model

In this study, we propose to model the AF or media of arterial tissue as a fiber-reinforced composite of which the fibers have a crimped microstructure. The AF and media of arterial tissues consist of several concentric lamellae, with the collagen fibers of each individual lamina being arranged in parallel. This model takes into account the dispersion of the fibers in different families and considers fiber waviness as a sinusoidal shape. Furthermore, in our assumption, the collagen fibers are only corrugated within the plane of the lamella. The proposed analytical solution is based on the effective stiffness matrix of composite reinforced with fibers of a particular sinusoidal waviness, as proposed by Xiao et al. [44] for the unique direction of fibers, and three-dimensional effective moduli of laminate composite proposed by Sun and Li [45] which helps us to take in account the different families of fibers.

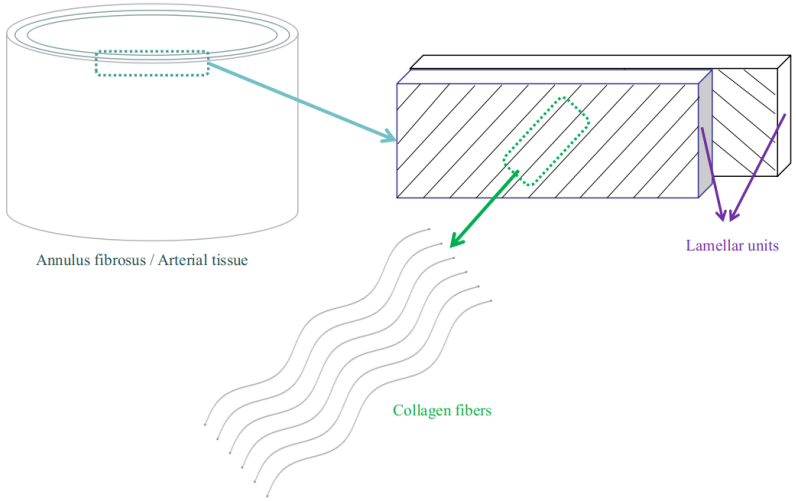

Figure 1: Scheme of AF or arterial tissue components and microstructure.

2.1 Composite reinforced with straight fibers

In order to develop our model, we first present an analytical solution based on the Eshelby equivalent inclusion method [46] for a stiffness matrix of composite reinforced with straight fibers.

The mechanical strain interaction between the fibers and matrix that make up a composite reinforced with straight fibers, based on the Eshelby equivalent inclusion method, can be expressed as

$$\hat{\varepsilon}_f = B : \hat{\varepsilon}_m, \tag{1}$$

where $\hat{\varepsilon}_f$ and $\hat{\varepsilon}_m$ are the average strain tensors in the fibers and matrix, respectively, and B is the concentration tensor whose details can be found in Parnell's monograph [47], which can be expressed as

$$B = [I + (S^E : S^m) : (C^f - C^m)]^{-1}, \tag{2}$$

where I is the identity tensor, C^f and C^m are the elastic stiffness tensors of isotropic fiber and matrix, respectively, S^m is the elastic compliance of the isotropic matrix ($S^m = [C^m]^{-1}$), and S^E is the Eshelby tensor.

The average stress of fibers $\hat{\sigma}_f$ is

$$\hat{\sigma}_f = C^f : \hat{\varepsilon}_f = C^f : B : \hat{\varepsilon}_m. \tag{3}$$

The average stress and strain tensors in the composite reinforced with straight fibers can be written in terms of matrix average stress $\hat{\sigma}_m$ as

$$\bar{\sigma} = V_m\hat{\sigma}_m + V_f\hat{\sigma}_f = V_m\hat{\sigma}_m + V_f C^f : B : \hat{\varepsilon}_m = V_m\hat{\sigma}_m + V_f C^f : B : (S^m : \hat{\sigma}_m), \tag{4}$$

$$\bar{\varepsilon} = V_m\hat{\varepsilon}_m + V_f\hat{\varepsilon}_f = V_m(S^m : \hat{\sigma}_m) + V_f B : (S^m : \hat{\sigma}_m), \tag{5}$$

where V_f and V_m are the volume fractions of the fibers and the matrix, respectively.

From Equations 4 and 5, the compliance matrix $\bar{S}$ of the composite reinforced with straight fibers can be obtained as

$$\bar{S} = (V_m I + V_f B) : (V_m C^m + V_f C^f : B)^{-1}. \tag{6}$$

For the composite reinforced with straight fibers, which are parallel to the x-axis, details can be found in the Mura's monograph [48]. By reformulating the axis, the nonzero components of the Eshelby tensor S^E are S^E_{2222}, S^E_{3333}, S^E_{2233}, S^E_{3322}, S^E_{2211}, S^E_{3311}, S^E_{2323}, and S^E_{1212}.

Inserting the Eshelby tensor into Equation 6, we get the equivalent compliance matrix for straight-fiber-reinforced composite $\bar{S}$ with the following formula, where the details of each nonzero component can be found in Xiao et al. [44]

$$\left[\bar{S}_{ij}\right] = \begin{bmatrix} \bar{S}_{11} & \bar{S}_{12} & \bar{S}_{12} & 0 & 0 & 0 \\ \bar{S}_{12} & \bar{S}_{22} & \bar{S}_{23} & 0 & 0 & 0 \\ \bar{S}_{12} & \bar{S}_{23} & \bar{S}_{22} & 0 & 0 & 0 \\ 0 & 0 & 0 & 2(\bar{S}_{22} - \bar{S}_{23}) & 0 & 0 \\ 0 & 0 & 0 & 0 & \bar{S}_{66} & 0 \\ 0 & 0 & 0 & 0 & 0 & \bar{S}_{66} \end{bmatrix}. \tag{7}$$

2.2 Composite reinforced with crimped fibers

Here, we present the analytical solution to finding the effective stiffness matrix $\hat{C}^{sin}_{ij}$ $(i, j = 1, 2, 3, 4, 5, 6)$ of composite reinforced with fibers of a particular sinusoidal shape [44], as shown in Figure 2(a). The fiber corrugation is assumed to be planar sinusoidal in the x-z plane and the corrugated fiber is shown in Figure 2(b) with Cartesian coordinates. Here, β represents the tangent angle of the sinusoidal fiber.

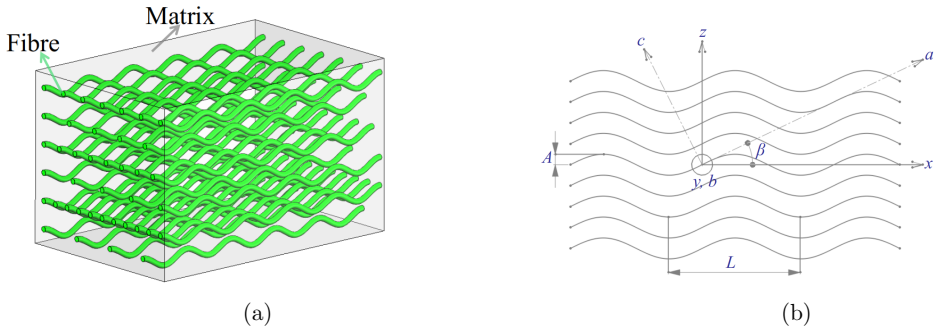

(a) (b)

Figure 2: (a) Composite reinforced with fibers of uniform sinusoidal waviness. (b) Corrugated fibers and Cartesian coordinates.

The crimped fiber shape is defined as

$$z = Asin(\frac{2\pi}{L}x), \tag{8}$$

where A is the amplitude and L represents the wavelength of the wavy fiber as shown in Figure 2(b).

The average transformed inverse compliance matrix $\hat{S}_{ij}^{sin}$ is obtained by integrating the compliance matrix $\bar{S}$ along one wavelength of the sinusoidal shape in the x-direction as (see the details in Hsiao et al. [49])

$$\hat{S}_{ij}^{sin}(\beta(A,L)) = \int_0^L \hat{S}_{ij}(\beta(A,L))dx, \tag{9}$$

where

$$\left[\hat{S}_{ij}\right] = \left[R_{ij}\right]\left[T_{ij}^{sin}\right]^{-1}\left[R_{ij}\right]^{-1}\left[\bar{S}_{ij}\right]\left[T_{ij}^{sin}\right], \tag{10}$$

and $\beta = arctan(\frac{2\pi A}{L}cos(\frac{2\pi}{L}x))$ and $x \in [0, L]$.
T_{ij}^{sin} is the general transformation matrix expressed as

$$\left[T_{ij}^{sin}\right] = \begin{bmatrix} cos^2(\beta(x)) & 0 & sin^2(\beta(x)) & 0 & 2cos(\beta(x))sin(\beta(x)) & 0 \\ 0 & 1 & 0 & 0 & 0 & 0 \\ sin^2(\beta(x)) & 0 & cos^2(\beta(x)) & 0 & -2cos(\beta(x))sin(\beta(x)) & 0 \\ 0 & 0 & 0 & cos(\beta(x)) & 0 & -sin(\beta(x)) \\ -sin(\beta(x))cos(\beta(x)) & 0 & sin(\beta(x))cos(\beta(x)) & 0 & cos^2(\beta(x)) - sin^2(\beta(x)) & 0 \\ 0 & 0 & 0 & sin(\beta(x)) & 0 & cos(\beta(x)) \end{bmatrix}, \tag{11}$$

and R_{ij} can be expressed as

$$\left[R_{ij}\right] = \begin{bmatrix} 1 & 0 & 0 & 0 & 0 & 0 \\ 0 & 1 & 0 & 0 & 0 & 0 \\ 0 & 0 & 1 & 0 & 0 & 0 \\ 0 & 0 & 0 & 2 & 0 & 0 \\ 0 & 0 & 0 & 0 & 2 & 0 \\ 0 & 0 & 0 & 0 & 0 & 2 \end{bmatrix}. \tag{12}$$

We then have

$$\left[\hat{C}_{ij}^{sin}\right] = \left[\hat{S}_{ij}^{sin}\right]^{-1}. \tag{13}$$

The nonzero element of matrix $\hat{S}_{ij}^{sin}$ can be expressed as

$$\left[\hat{S}_{ij}^{sin}\right] = \begin{bmatrix} \hat{S}_{11}^{sin} & \hat{S}_{12}^{sin} & \hat{S}_{13}^{sin} & 0 & 0 & 0 \\ \hat{S}_{12}^{sin} & \hat{S}_{22}^{sin} & \hat{S}_{23}^{sin} & 0 & 0 & 0 \\ \hat{S}_{13}^{sin} & \hat{S}_{23}^{sin} & \hat{S}_{33}^{sin} & 0 & 0 & 0 \\ 0 & 0 & 0 & \hat{S}_{44}^{sin} & 0 & 0 \\ 0 & 0 & 0 & 0 & \hat{S}_{55}^{sin} & 0 \\ 0 & 0 & 0 & 0 & 0 & \hat{S}_{66}^{sin} \end{bmatrix}. \tag{14}$$

2.3 Composite reinforced with crimped fibers with alternatively oriented layers

We propose an analytical solution that takes into account the multiple layers and the relative orientation of each layer to find the effective elastic stiffness matrix. To do so, single-layer solutions are also presented.

2.3.1 Single layer of the multilayered composite

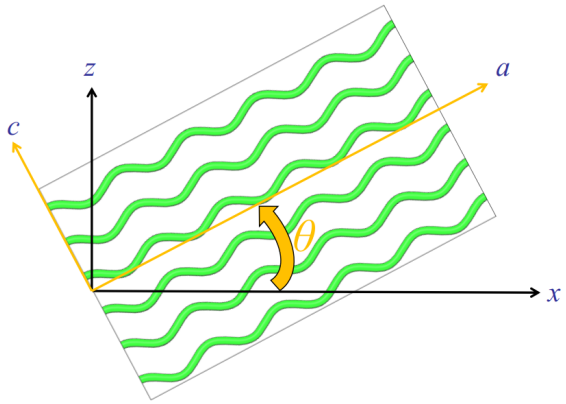

Figure 3: Composite orientation in the Cartesian coordinate system.

One layer, or "lamella" of the composite reinforced with fibres of uniform sinusoidal waviness is rotated by an angle of θ around the y-axis as shown in Figure 3. The effective stiffness matrix of this layer $\tilde{C}_{ij}^{layer1}$ and its inverse compliance $\tilde{S}_{ij}^{layer1}$ can be deduced as

$$\left[\tilde{S}_{ij}^{layer1}\right] = \left[R_{ij}\right]\left[T_{ij}^{st}\right]^{-1}\left[R_{ij}\right]^{-1}\left[\hat{S}_{ij}^{sin}\right]\left[T_{ij}^{st}\right] \qquad \left[\tilde{C}_{ij}^{layer1}\right] = \left[\tilde{S}_{ij}^{layer1}\right]^{-1}, \tag{15}$$

where the general transformation matrix T_{ij}^{st} is

$$\left[T_{ij}^{st}\right] = \begin{bmatrix} cos^2(\theta) & 0 & sin^2(\theta) & 0 & 2cos(\theta)sin(\theta) & 0 \\ 0 & 1 & 0 & 0 & 0 & 0 \\ sin^2(\theta) & 0 & cos^2(\theta) & 0 & -2cos(\theta)sin(\theta) & 0 \\ 0 & 0 & 0 & cos(\theta) & 0 & -sin(\theta) \\ -sin(\theta)cos(\theta) & 0 & sin(\theta)cos(\theta) & 0 & cos^2(\theta) - sin^2(\theta) & 0 \\ 0 & 0 & 0 & sin(\theta) & 0 & cos(\theta) \end{bmatrix}. \tag{16}$$

The nonzero element of matrix $\tilde{S}_{ij}^{layer1}$ can be expressed as

$$\left[\tilde{S}_{ij}^{layer1}\right] = \begin{bmatrix} \tilde{S}_{11}^{layer1} & \tilde{S}_{12}^{layer1} & \tilde{S}_{13}^{layer1} & 0 & \tilde{S}_{15}^{layer1} & 0 \\ \tilde{S}_{12}^{layer1} & \tilde{S}_{22}^{layer1} & \tilde{S}_{23}^{layer1} & 0 & \tilde{S}_{25}^{layer1} & 0 \\ \tilde{S}_{13}^{layer1} & \tilde{S}_{23}^{layer1} & \tilde{S}_{33}^{layer1} & 0 & \tilde{S}_{35}^{layer1} & 0 \\ 0 & 0 & 0 & \tilde{S}_{44}^{layer1} & 0 & \tilde{S}_{46}^{layer1} \\ \tilde{S}_{15}^{layer1} & \tilde{S}_{25}^{layer1} & \tilde{S}_{35}^{layer1} & 0 & \tilde{S}_{55}^{layer1} & 0 \\ 0 & 0 & 0 & \tilde{S}_{46}^{layer1} & 0 & \tilde{S}_{66}^{layer1} \end{bmatrix}. \tag{17}$$

2.4 Multiple layers

Here, we introduce an analytical approach to finding the effective elastic stiffness tensor of a composite composed of several layers by applying formulations given in [45]. Each considered layer, or lamella, is a composite reinforced with fibers of uniform sinusoidal waviness. The coordinate system is set so that the x- and z-axes lie in the plane of the lamella and the y-axis is perpendicular to that plane. The laminate composite contains r orthotropic fiber-composite layers and each layer is rotated by a corresponding angle $\theta_k (k = 1, 2, 3 \cdots)$ around the y-axis as shown in Figure 4(a).

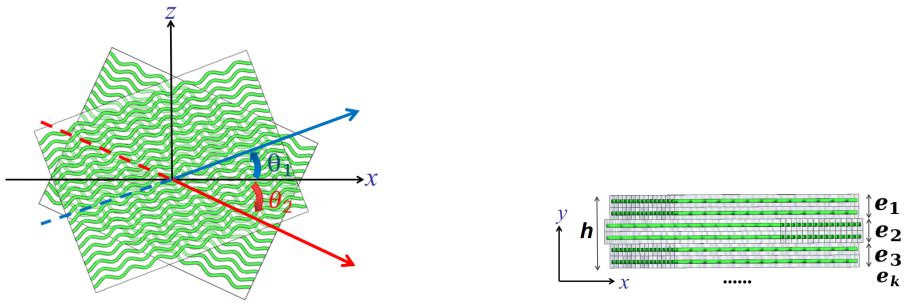

(a) (b)

Figure 4: Organization of the synthetic laminate (a) Multilayer laminate with coordinate system. Two lamellae are shown: the first and second lamellae are orientated by θ_1 and θ_2 around the y-axis with respect to the x-axis, respectively. (b) Schema of laminate total thickness h, and thickness of each layer $e_k (k = 1, 2, 3 \cdots)$.

The effective macro-stresses σ^{total} and macro-strains ε^{total} are defined as

$$\sigma_{ij}^{total} = \frac{1}{V} \int_V \sigma_{ij} dV, \tag{18}$$

and

$$\varepsilon_{ij}^{total} = \frac{1}{V} \int_V \varepsilon_{ij} dV, \tag{19}$$

where V is the volume that contains the total thickness of the lamellae.

The in-plane dimensions are kept infinitesimal so that the stresses and strains in each layer are uniform in the planar directions. As the stresses and strains in each lamella are constant, Equations 18 and 19 can be integrated as

$$\sigma_{ij}^{total} = \sum_{k=1}^{r} V_k (\sigma_{ij})_k, \tag{20}$$

and

$$\varepsilon_{ij}^{total} = \sum_{k=1}^{r} V_k (\varepsilon_{ij})_k, \tag{21}$$

where $(\sigma_{ij})_k$ and $(\varepsilon_{ij})_k$ are the stresses and strains in the kth $(k = 1, 2, 3 \cdots)$ layer, and

$$V_k = \frac{e_k}{h}, \tag{22}$$

where e_k is the thickness of the kth lamella, and h is the total thickness of the laminate as shown in Figure 4(b).

We assume that the strain of each layer along the x-axis and z-axis is equal to the global strain of the multi-layer laminate along the x-axis and z-axis, respectively. Additionally, we assume that the stress on each layer along the y-axis is the same as the global stress along the y-axis. Thus, the terms of the stress and strain conditions are assumed as follows:

$$\begin{cases} (\varepsilon_{xx})_k = \varepsilon_{xx}^{total} \\ (\varepsilon_{zz})_k = \varepsilon_{zz}^{total} \\ (\gamma_{xz})_k = \gamma_{xz}^{total} \\ (\sigma_{yy})_k = \sigma_{yy}^{total} \\ (\sigma_{xy})_k = \sigma_{xy}^{total} \\ (\sigma_{yz})_k = \sigma_{yz}^{total} \end{cases}. \tag{23}$$

The effective elastic stiffness matrix of the multilayer laminate $\tilde{C}_{ij}^{total}$ can be expressed as

$$\left[\tilde{C}_{ij}^{total}\right] = \begin{bmatrix} \tilde{C}_{11}^{total} & \tilde{C}_{12}^{total} & \tilde{C}_{13}^{total} & 0 & \tilde{C}_{15}^{total} & 0 \\ \tilde{C}_{12}^{total} & \tilde{C}_{22}^{total} & \tilde{C}_{23}^{total} & 0 & \tilde{C}_{25}^{total} & 0 \\ \tilde{C}_{13}^{total} & \tilde{C}_{23}^{total} & \tilde{C}_{33}^{total} & 0 & \tilde{C}_{35}^{total} & 0 \\ 0 & 0 & 0 & \tilde{C}_{44}^{total} & 0 & \tilde{C}_{46}^{total} \\ \tilde{C}_{15}^{total} & \tilde{C}_{25}^{total} & \tilde{C}_{35}^{total} & 0 & \tilde{C}_{55}^{total} & 0 \\ 0 & 0 & 0 & \tilde{C}_{46}^{total} & 0 & \tilde{C}_{66}^{total} \end{bmatrix}. \tag{24}$$

The nonzero elements of $\tilde{C}_{ij}^{total}$ can be obtained from Equations 20, 21, and 23 (see the details of the developments limited to straight fibers in Sun et al. [45]).

The effective elastic compliance matrix of a multilayered composite $\tilde{S}_{ij}^{total}$ is

$$[\tilde{S}_{ij}^{total}] = [\tilde{C}_{ij}^{total}]^{-1}. \tag{25}$$

3 Material parameter study

We consider the lamellar structure in AF or arterial tissue as a composite reinforced with corrugated fibers and study its mechanical behavior by applying the proposed micromechanical model. Our parameter study is based on data reported in the literature. The elastic modulus of collagen has been reported at different scales, from molecular to whole tissues, revealing that the mechanical stiffness decreases as the hierarchy scale increases; in other words, $E_{monomer} > E_{fibril} > E_{fiber} > E_{tissue}$ [50]. Although the collagen elastic modulus is most often reported at the lamella scale [51][52], there are a few examples in the literature of the elastic modulus studied at the single collagen fiber scale. Ambard and Cherblanc [53] showed the collagen fiber elastic modulus to range from $6.6MPa$ to $12.3MPa$ using a tensile test on lamb and pig annulus fibrosus tissues as part of their development of a rheological model. Also, the collagen Type I single-fiber elastic modulus was measured between 100 MPa and 360 MPa in rat tail tendon using an approach that combines optical tweezers, atomic force microscopy, and exploitation of Euler-Bernoulli elasticity theory [54]. Type I collagen fibers are the most prevalent fibers [55] in AF, and the type III collagen fiber is the most abundant collagen type in arterial tissue, although type I collagen is also present here in significant amounts [56]. We consider that the measured collagen fiber modulus for type I collagen reported by Dutov et al. [54] can also be applied in our study. The mechanical properties of the ground matrix of bovine AF were measured by Cortes et al. using tensile and confined compression tests, revealing an aggregate modulus of $10.18 \pm 3.32KPa$ [57]. As the arterial tissue contains amounts of smooth muscle cells (SMCs) in the ground substance, we consider the elastic modulus of SMCs as the elastic modulus of the matrix, which is reported to be about $10KPa$ by Nagayama et al. from rat thoracic aortas [58]. The fiber volume fractions have been found to range from 0.05 to 0.245 based on the description that AF comprises 65%–90% wet weight (water) and 50%—70% dry weight (collagen) [59]. Collagen recruitment was reported to be $10 \pm 1\%$ in rat abdominal aorta by O'Connell et al. [60]. The Poisson's ratios of the fiber (0.3) and matrix (0.4) used in our

study are based on a previous modeling study, which is summarized by Sharabi et al. [55]. The fiber orientation in the circumferential direction varies between lamellae by 25° to 45° reported by Baldit et al. [61]in porcine AF and ±10° in the aortic medial [60]. The individual medial lamellar unit measured $13.9 \pm 1.2 \mu m$ for the aortic medial [60] measured 0.14 - 0.52 mm in the lateral portion and inner layers of the AF [62]. The crimp level of collagen fibers, represented by $\frac{A}{L}$, is assumed to vary between 0.08 and 0.25. This variation is based on the description provided by Sharabi [63], where it is stated that the crimp angle increases from 20° to 45°. The crimp angle is determined by taking the arctan of the sinusoidal amplitude divided by a quarter sinusoidal period. Furthermore, the porcine AF consists of 7 - 25 lamellae [62][61] and rat abdominal aorta contains about 8 lamellae [60]. The parameters used in our study are summarized in Table 1.

Parameter	Meaning	Value
E_f	Collagen fiber modulus	100 MPa
E_m	Extracellular matrix modulus	10 KPa
V_f	Collagen fiber volume fraction	0.2
V_m	Matrix volume fraction	0.8
ν_f	Collagen fiber Poisson's ratio	0.3
ν_m	Extracellular matrix Poisson's ratio	0.4
θ	Layer orientation angle	0° - 90°
$\frac{A}{L}$	Collagen fiber crimp level	0.01 - 0.3
e_k	Thickness of each layer	0.5 mm
r	Number of layers	1, 2, 10

Table 1: Parameters used in our study. Please note the wide ranges for layer orientation angle, fiber crimp level, and number of layers (i.e., families of fibers).

4 Results

In this section, the effects of fiber crimp level, layer orientation angle, and number of layers on the Poisson's ratio of the fibrous-tissue-like composite are quantified using a theoretical analysis. The effective Poisson's ratio for a laminate of one or multiple layers is obtained from $\tilde{S}_{ij}$ (here, $\tilde{S}_{ij}$ represents $\tilde{S}_{ij}^{layer1}$ or $\tilde{S}_{ij}^{total}$ according to the particular application) as:

$$\nu_{xy} = -\frac{\tilde{S}_{21}}{\tilde{S}_{11}} \qquad \nu_{xz} = -\frac{\tilde{S}_{31}}{\tilde{S}_{11}}, \tag{26}$$

where the term ν_{ij} is the effective Poisson's ratio, which characterizes the strain in the j direction produced by the loading in the i direction.

4.1 Single and double layer

In this section, we compare the difference in Poisson's ratio between a single layer (i.e., a single family of fibers) and a double layer (i.e., two families of fibers). The values of the model parameters are shown in Table 1. For the double-layer analysis, the two layers are set to have the same thickness of 0.5 mm ($e_1 = e_2$), and the orientation of the first and second layers is symmetrical on either side of the x-axis, which means $\theta_1 = -\theta_2$. With these parameters, the model is able to predict the effective Poisson's ratio as functions of fiber crimp level ($0.01 < \frac{A}{L} < 0.3$) and layer orientation angle ($0° < \theta < 90°$).

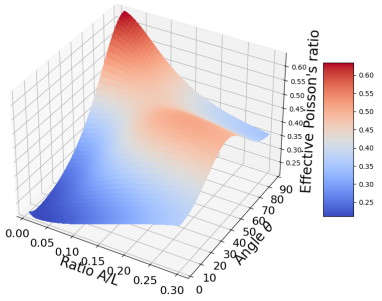

Single layer ν_{xy}
(a)

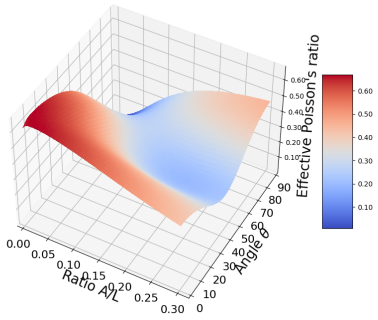

Single layer ν_{xz}
(b)

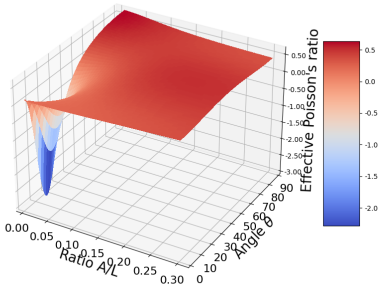

Double layer ν_{xy}
(c)

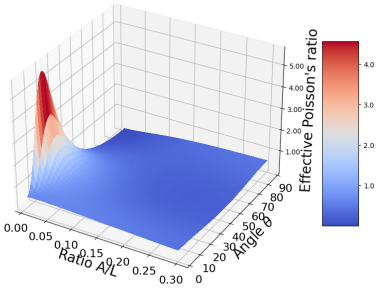

Double layer ν_{xz}
(d)

Figure 5: Poisson's ratio under the loading along the x-direction for single- (a)(b) and double-layer composite (c)(d) as a function of fiber crimp level $\frac{A}{L}$ and layer orientation θ. See the value settings for the parameters in Table 1.

Figure 5 shows how the effective Poisson's ratios ν_{xy} and ν_{xz} vary with changes to fiber crimp level $\frac{A}{L}$ and layer orientation θ for single- and double-layer composites. For the single-layer composite, ν_{xy} and ν_{xz} are affected by both $\frac{A}{L}$ and θ. Interestingly, ν_{xy} and ν_{xz} show opposite trends with changes to $\frac{A}{L}$ and θ as shown in Figure 5 (a) and (b). When $\frac{A}{L}$ is small and θ is large, the effective Poisson's ratio ν_{xz} has a minimum value of 0.004 and the effective Poisson's ratio ν_{xy} has a maximum value of 0.63. For the fiber crimp level ($0.08 < \frac{A}{L} < 0.25$) and orientation angle ($25° < \theta < 45°$) in the physiological range of AF, the values of ν_{xy} and ν_{xz} are neither negative nor larger than 0.5. For quasi-straight fibers ($\frac{A}{L} < 0.05$), we find a Poisson's ratio ν_{xz} of over 0.6. For a double-layer composite with the two layers arranged symmetrically on the x-axis, ν_{xy} and ν_{xz} are also affected by both $\frac{A}{L}$ and θ. Moreover, ν_{xy} and ν_{xz} also show opposite trends with changes to $\frac{A}{L}$ and θ, as shown in Figure 5 (c) and (d). As opposed to the single-layer composite, a negative Poisson's ratio value for ν_{xy} and a Poisson's ratio of greater than 0.5 for ν_{xz} are observed for double-layer composite. When the fiber is almost straight ($\frac{A}{L} < 0.05$) the effective Poisson's ratio ν_{xy} has a minimum value of -3.0 and ν_{xz} has a maximum value of 5.7 when $\theta_1 = -\theta_2 = 17$ ° in this study. Note that the angle θ at which both ν_{xy} and ν_{xz} reach their limit values is influenced by the ratio of stiffness between the fiber and the

matrix. A decrease in the ratio $\frac{E_f}{E_m}$ results in an increase in the angle θ at which the limit values occur. For fiber crimp levels ($0.08 < \frac{A}{L} < 0.25$) and orientation angles ($25° < \theta < 45°$) in the physiological range of AF, the values of ν_{xz} are usually larger than those of ν_{xz}, which is in good agreement with the observations in the literature [12]; when subjected to loading in the circumferential direction, the Poisson's ratio characterizing the strain in the radial direction is typically much lower than the Poisson's ratio characterizing the strain in the longitudinal direction. Additionally, with the extension of AF tissue in the circumferential direction, an expansion in the radial direction is observed in some cases [9].

4.2 Ten-layer laminate

In this analysis, we study the effective mechanical properties of a composite model with ten layers ($r = 10$) as a function of the relative orientation of the successive layers and fiber crimp level; a laminate schematic diagram and the coordinate system are shown in Figure 4, where the x- and z-axes lie in the plane of the lamella and the y-axis is perpendicular to that plane, and the layer orientation angle settings are shown in Table 2. We note that the properties of the ten-layer symmetrically arranged laminate with the constant angle between successive layers are exactly the same as those of the two-layer laminate. In cases 1 and 2, the average orientation angle of ten layers is $|40°|$, and in case 1, a wider range of orientation angles is tested. In case 3, the orientation angle is set at a constant 40° between successive layers $|\theta_k|$ =40°, (k = 1, 2, 3 $\cdots$). In case 4, the orientation angles increase from one layer to the next with a constant step of 18° degrees. The thickness of each layer is set to 0.5 mm. These parameters predict the effective Poisson's ratio as a function of the orientation of the successive layers as well as fiber crimp level in the range $0.01 < \frac{A}{L} < 0.3$, as shown in Figure 6.

Layer number	θ_1	θ_2	θ_3	θ_4	θ_5	θ_6	θ_7	θ_8	θ_9	θ_{10}
Case 1	20°	-20°	30°	-30°	40°	-40°	50°	-50°	60°	-60°
Case 2	30°	-30°	35°	-35°	40°	-40°	45°	-45°	50°	-50°
Case 3	40°	-40°	40°	-40°	40°	-40°	40°	-40°	40°	-40°
Case 4	0°	18°	36°	54°	78°	90°	108°	126°	144°	162°

Table 2: Layer orientation angle settings for each of the ten lamellae of the model. Four cases are studied.

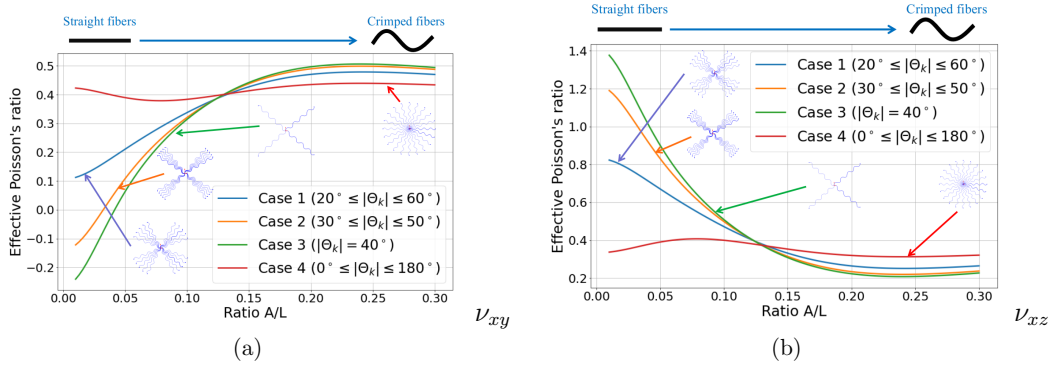

ν_{xy} (a) ν_{xz} (b)

Figure 6: Effective Poisson's ratios (a) ν_{xy}, (b) ν_{xz} for a ten-layer laminate model as a function of fiber crimp level and relative orientation of the successive layers of the laminate model. See the value settings for the parameters in Table 1.

Figure 6 shows how the effective Poisson's ratios ν_{ij} of a ten-layer laminate model vary with changes to fiber crimp level $\frac{A}{L}$ in the laminate as a whole and changes to orientation angle between each of its ten successive layers (or no change, as in case 3). The behavior of the Poisson's ratios in cases 1 and 2 is the same as that of case 3 where the orientation angle between successive layers is constant. Each effective ν_{ij} value in case 2 is always between the values of cases 1 and 3 at each increment in $\frac{A}{L}$, which indicates that the trend seen for the Poisson's ratios is that the larger the range of layer orientation angles in the laminate, the larger the difference between the global effective Poisson's ratio and the constant average case Poisson's ratio. Moreover, we observe a negative Poisson's ratio ν_{xy} in case 3, but not in case 1, which shows that variation in the orientation between successive layers could also weaken the auxetic response. In case 4, where the ten fiber families are regularly oriented and collectively span 180°, the Poisson's ratios ν_{xy} and ν_{xz} are between 0.3 and 0.5, canceling all the effects found for two fiber families oriented at 40°. We conclude that only tissues with just two distinct orientations of fibers can have negative apparent Poison's ratios. We note that, in our parameter studies, not shown here, we also found that the minimum value of the Poisson's ratio ν_{xy} and the maximum value of the Poisson's ratio ν_{xz} vary as the Poisson's ratio of the matrix changes. Modification of the Poisson's ratio of the matrix from 0.4 to 0.1 induces a change in the effective Poisson's ratio ν_{xy} from -3.0 to -0.85. Moreover, the orientation angle θ for which ν_{xy} has the minimum value changes with modification of the elastic modulus ratio E_f/E_m.

5 Discussion and conclusions

In this paper, we use an analytical micromechanical model to study the effective Poisson's ratio of the lamellar-composite-like structure of fibrous tissue, with a focus on the roles of the orientation angle between the parallel fibers of successive lamellae and the corrugation (or crimp level) of those fibers. Xiao et al. [44] proposed an analytical model to study the tendon tissue that is based on an Eshelby tensor and takes into account the waviness of fibers. The originality of the method used by these latter authors is that it can be used to predict — without any strong assumptions, for example as to the equality of the deformation between phases — the relationship between the deformation of the fibers and the deformation of the matrix. However, the model used by Xiao et al. [44] is limited to unidirectional fibers. Hsiao et al. [49] proposed an interesting 2D approach similar to that of Xiao et al., to take into account the waviness of fibers in different directions. However, a significant assumption is required as part of this 2D approach, namely that fibers and matrix have the same deformation, which limits the versatility of the model and the conclusions that can be drawn from it. Based on the method presented by Sun and Li [45], we propose an original 3D model that, without any strong assumptions as to the affinity between the fibers and the matrix (no equality between their deformation), merges the 2D multidirectional model of Hsiao et al. [49] with the 3D unidirectional wavy model of Xiao et al [44].

Our proposed micromechanical model can be used to quickly estimate the small strain mechanical properties of a composite laminate embedded with crimped fibers of alternate orientation between layers using theoretical calculations only. Our model can easily be used to analyze the influence of crimp level and relative fibre orientation on the effective mechanical properties of the modeled material. The modulus of fiber E_f and matrix E_m, the Poisson's ratios of fiber ν_f and matrix ν_m, the volume fraction of the fibers V_f and matrix V_m, fiber crimp level $\frac{A}{L}$, the relative fibre orientation angle of successive layers θ_k, layer thickness e_k, and total number of layers r are taken into account as parameters potentially modifying the mechanical properties of the laminate. The model described is designed to mimic, and therefore allows us to study, the morphological aspects of AF and arterial wall, but the approaches and techniques employed are also applicable to other fiber-reinforced biological tissues and biocomposites.

For a single-layer composite, ν_{xy} and ν_{xz} are affected by both fiber crimp level $\frac{A}{L}$ and layer

orientation θ. For a two-layer laminate, the range of ν_{ij} is significantly expanded: the minimum value is even negative and the maximum value is 5.7. It is known that, for isotropic solids, the Poisson's ratio is in general smaller than 0.5, but the Poisson's ratio in certain microstructures of the composites under study can be significantly larger than 0.5, as shown in Figure 5. This is because of the effects of corrugated fibers and alternately oriented layers. As fibers are considered slightly corrugated, when the dispersed fibers are stretched, the fiber–matrix stiffness ratio causes the matrix between the fibers to be compressed, which can lead to expansion in the x-y plane. Similar observations were reported based on analytical analyses [64][45], numerical simulation studies [43][2], and tensile experiments on AF or arterial tissue [8] [9][12][26][25][29].

The proposed model could explain the negative Poisson's ratios found for AF or media of arterial tissue in the plane perpendicular to that of the fibers. Moreover, our analytical model confirms that just two fiber directions (not one, not three, etc) may confer an auxetic behavior in the plane perpendicular to the direction of fibers ($\nu_{xy} < 0$), while multiplying the number of different fiber directions reduces this auxetic behavior. The same phenomenon is demonstrated for the Poisson's ratio ν_{xz} along the mean orientation of the fibres, with very high values possible when there are only two families of fibers, which fades when multiplying the fiber orientations. We note that our analytical model predicts that there must be an inter-fibrilar medium with finite compressibility in order to to see such transverse behaviors. Moreover, as $\frac{A}{L}$ increases, the negative Poisson's ratios gradually disappear, that is to say that one of the mechanical effects of the corrugated fibers in the microstructure of the laminate model studied here is to reduce its auxetic behavior. In conclusion, because of the fiber–matrix stiffness ratio and fiber dispersion, the laminate composite shows an auxetic behavior in the planes perpendicular to the plane of the fibers. However, this behavior is not easily measured because of the joint influence of fiber crimp level and successive layer orientation. Therefore, the present work provides evidence of the link between corrugated fiber structure and auxetic behavior, which answers speculation in the literature. Furthermore, compared to the well-known HGO constitutive model [15] or HGO-based models in the literature, which often observe out-of-plane expansion, this work could be a solution to avoid the auxetic response in modeling from the perspective of fiber microstructure.

Our study focuses solely on the linear behavior of corrugated fiber composites. Our model may be completed to describe non-linear composite behaviors. However, provided the microstructure is stable (e.g. no micro-buckling or micro-fractures), our linear model may predict the behavior of such composite for finite strains. Classically admitted and shown for the arterial tissue, the crimp level of the fibers is higher when the tissue is not stretched than when it's stretched. Our model would therefore predict a positive Poisson's ratio for low deformation when the fibers are undulated (i.e. for large A/L), and either a negative Poisson's ratio (theta-r plan) or a large Poisson's ratio (theta-z plan) for higher deformations when the fibers are straight due to stretching (i.e. low A/L). For AF tissue, this point seems to be in agreement with experimental measurements made by Dusfour et al.[9] in the laminate plan, but not out of the laminate plan. In this study, for the laminate plan, the Poisson's ratio increases with the circumferential stretch, reaching elevated values, as our linear model could predict. However, in the plan out of the laminate, their study shows that the samples are not auxetic beyond 4% circumferential strain which is not in agreement with our model. For arterial tissues, no measures of non-linear Poisson's ratios have been made to our knowledge. Thus, to link our model to experimental observations, we need to increase our knowledge on the evolution of the microstructure (and especially the crimp level) with macroscopic finite strains. Our model should also be completed to link the crimp level with the macroscopic deformation, which is not straightforward.

The present study is limited to testing the effects of small strains on the laminate material, which is considered as a linear elastic behavior. It is also noted that the [46] Eshelby equivalent inclusion method provides the best estimation when the fiber volume fractions are relatively low (below 60%) [65][66][67]. The fiber volume fraction of AF or arterial tissue is estimated to be much less than 60%. Therefore, we consider the Eshelby method to be suitable for use

in conjunction with the proposed model, but for other applications, the limits of fiber volume fraction should be reconsidered and an alternative method for estimation of fiber volume fraction may be needed. Moreover, in our model, the strain of each layer along the x-axis and z-axis is assumed to be equal to the global strain of the multi-layer laminate along the x-axis and z-axis, respectively, and the stress on each layer along the y-axis is assumed to be the same as the global stress along the y-axis, as shown in Equation 23. However, no accepted method exists at present to verify these assumptions for AF and arterial tissues. Indeed, our model is not designed to predict how the Poisson's Ratio varies throughout the thickness of these structures. Furthermore, we have considered the fibers to be corrugated only in the plane of the lamella. However, recent evidence [68] suggests that collagen fibers in the AF may also exhibit crimped properties in the plane perpendicular to the lamella plane, which has not been taken into account in this study. Although the macroscopic properties of AF and arterial tissues are well established in the literature, the link between their macroscopic behavior and microscopic structure still needs to be elucidated. Our study provides a method for predicting the macroscopic properties of fibrous soft tissues based on their fiber microstructure. It is noted that, here, the AF and arterial tissues are considered to be composite-like materials composed of fibers and solid matrix. Although Derrouiche et al.'s [12] research shows that the auxetic behavior of AF is related to the osmolarity of the liquid phase, Dusfour et al.'s [9] research suggests that the auxetic behavior may be primarily influenced by the solid structure. This is because they conducted their experiments under steady-state stretching conditions, thus excluding the influence of the viscous and dynamic effects of the liquid phase. In our study, the fiber and matrix are considered as compressible solid phases; however, the structure and composition of real arterial tissue and AF are much more complex. By nature, our homogenization method requires precise knowledge of the mechanical behaviors of each component of the tissue under study. In order to make better use of our model, further characterization of the different components of the microstructure of the studied tissue is also necessary.

6 Acknowledgements

We thank Pr. Loïc Daridon, Pr. Yann Monerie and Dr. Cristina Cavinato for the scientific discussions. This work was supported by CNRS (AAP "Osez l'Interdisciplinarité" and MoTiV Project).

References

[1] Yuan Jin, Chaoqi Xie, Qing Gao, Xueyong Zhou, Guangyong Li, Jianke Du, and Yong He. Fabrication of multi-scale and tunable auxetic scaffolds for tissue engineering. *Materials & Design*, 191:108641, 2020.

[2] Behrooz Fereidoonnezhad, C. O'connor, and JP McGarry. A new anisotropic soft tissue model for elimination of unphysical auxetic behaviour. *Journal of Biomechanics*, 111:110000, 2020.

[3] Dawn M Elliott, Dawn A Setton, et al. Anisotropic and inhomogeneous tensile behavior of the human anulus fibrosus: experimental measurement and material model predictions. *Journal of biomechanical engineering*, 123(3):256–263, 2001.

[4] Heather Anne L Guerin and Dawn M Elliott. Degeneration affects the fiber reorientation of human annulus fibrosus under tensile load. *Journal of biomechanics*, 39(8):1410–1418, 2006.

[5] Naama T Lewis, Mohammad A Hussain, and Jeremy J Mao. Investigation of nano-mechanical properties of annulus fibrosus using atomic force microscopy. *Micron*, 39(7):1008–1019, 2008.

[6] Grace D O'Connell, Heather L Guerin, and Dawn M Elliott. Theoretical and uniaxial experimental evaluation of human annulus fibrosus degeneration. 2009.

[7] Fabien Cherblanc, Dominique Ambard, Adrien Baldit, and JM Lafosse. Mechanical behaviour of annulus fibrosus: the role of the fluid phase. In *3rd International Conference on Porous Media*, pages Clé–USB, 2011.

[8] Adrien Baldit, Dominique Ambard, Fabien Cherblanc, and Pascale Royer. Experimental analysis of the transverse mechanical behaviour of annulus fibrosus tissue. *Biomechanics and modeling in mechanobiology*, 13(3):643–652, 2014.

[9] Gilles Dusfour, S LeFloc'h, Patrick Cañadas, and Dominique Ambard. Heterogeneous mechanical hyperelastic behavior in the porcine annulus fibrosus explained by fiber orientation: An experimental and numerical approach. *Journal of the mechanical behavior of biomedical materials*, 104:103672, 2020.

[10] EC Bass, FA Ashford, MR Segal, and JC Lotz. Biaxial testing of human annulus fibrosus and its implications for a constitutive formulation. *Annals of biomedical engineering*, 32(9):1231–1242, 2004.

[11] Grace D O'Connell, Sounok Sen, and Dawn M Elliott. Human annulus fibrosus material properties from biaxial testing and constitutive modeling are altered with degeneration. *Biomechanics and modeling in mechanobiology*, 11(3):493–503, 2012.

[12] Amil Derrouiche, Fahmi Zaïri, and Fahed Zaïri. A chemo-mechanical model for osmo-inelastic effects in the annulus fibrosus. *Biomechanics and modeling in mechanobiology*, 18(6):1773–1790, 2019.

[13] Diane R Wagner and Jeffrey C Lotz. Theoretical model and experimental results for the nonlinear elastic behavior of human annulus fibrosus. *Journal of orthopaedic research*, 22(4):901–909, 2004.

[14] Karim Kandil, Fahmi Zaïri, Amil Derrouiche, Tanguy Messager, and Fahed Zaïri. Interlamellar-induced time-dependent response of intervertebral disc annulus: A microstructure-based chemo-viscoelastic model. *Acta biomaterialia*, 100:75–91, 2019.

[15] Gerhard A Holzapfel, Thomas C Gasser, and Ray W Ogden. A new constitutive framework for arterial wall mechanics and a comparative study of material models. *Journal of elasticity and the physical science of solids*, 61(1):1–48, 2000.

[16] Han-Chin Wu and Ren-Feng Yao. Mechanical behavior of the human annulus fibrosus. *Journal of biomechanics*, 9(1):1–7, 1976.

[17] Robert Eberlein, Gerhard A Holzapfel, and Christian AJ Schulze-Bauer. An anisotropic model for annulus tissue and enhanced finite element analyses of intact lumbar disc bodies. *Computer methods in biomechanics and biomedical engineering*, 4(3):209–229, 2001.

[18] XQ Peng, ZY Guo, and B Moran. An anisotropic hyperelastic constitutive model with fiber-matrix shear interaction for the human annulus fibrosus. 2006.

[19] Doli J Patel, Joseph S Janicki, and Thomas E Carew. Static anisotropic elastic properties of the aorta in living dogs. *Circulation Research*, 25(6):765–779, 1969.

[20] RH Cox. Anisotropic properties of the canine carotid artery in vitro. *Journal of biomechanics*, 8(5):293–300, 1975.

[21] Hans W Weizsäcker, Helen Lambert, and Karin Pascale. Analysis of the passive mechanical properties of rat carotid arteries. *Journal of biomechanics*, 16(9):703–715, 1983.

[22] D Nahon, JM Lee, and GJ Wilson. A two-dimensional incremental study of the static mechanical properties of vascular grafts. *Clinical Materials*, 1(3):177–197, 1986.

[23] Hideyuki Hasegawa, Hiroshi Kanai, Noriyoshi Chubachi, and Yoshiro Koiwa. Non-invasive evaluation of poisson's ratio of arterial wall using ultrasound. *Electronics letters*, 33(4):340–342, 1997.

[24] Dongsheng Zhang, Charles D Eggleton, and Dwayne D Arola. Evaluating the mechanical behavior of arterial tissue using digital image correlation. *Experimental mechanics*, 42(4):409–416, 2002.

[25] MA Lillie, RE Shadwick, and JM Gosline. Mechanical anisotropy of inflated elastic tissue from the pig aorta. *Journal of biomechanics*, 43(11):2070–2078, 2010.

[26] Lucas H Timmins, Qiaofeng Wu, Alvin T Yeh, James E Moore Jr, and Stephen E Greenwald. Structural inhomogeneity and fiber orientation in the inner arterial media. *American Journal of Physiology-Heart and Circulatory Physiology*, 298(5):H1537–H1545, 2010.

[27] Y Liu, W Zhang, C Wang, and GS Kassab. A linearized and incompressible constitutive model for arteries. *Journal of theoretical biology*, 286:85–91, 2011.

[28] Alireza Karimi, Toshihiro Sera, Susumu Kudo, and Mahdi Navidbakhsh. Experimental verification of the healthy and atherosclerotic coronary arteries incompressibility via digital image correlation. *Artery Research*, 16:1–7, 2016.

[29] Pavel Skacel and Jiri Bursa. Poisson s ratio of arterial wall–inconsistency of constitutive models with experimental data. *Journal of the mechanical behavior of biomedical materials*, 54:316–327, 2016.

[30] Víctor A Acosta Santamaría, María Flechas García, Jérôme Molimard, and Stéphane Avril. Characterization of chemoelastic effects in arteries using digital volume correlation and optical coherence tomography. *Acta Biomaterialia*, 102:127–137, 2020.

[31] Pavel Skacel and Jiri Bursa. Poisson's ratio and compressibility of arterial wall–improved experimental data reject auxetic behaviour. *Journal of the Mechanical Behavior of Biomedical Materials*, 131:105229, 2022.

[32] Chavaunne T Thorpe, Graham P Riley, Helen L Birch, Peter D Clegg, and Hazel RC Screen. Effect of fatigue loading on structure and functional behaviour of fascicles from energy-storing tendons. *Acta biomaterialia*, 10(7):3217–3224, 2014.

[33] Ruben Gatt, Michelle Vella Wood, Alfred Gatt, Francis Zarb, Cynthia Formosa, Keith M Azzopardi, Aaron Casha, Tonio P Agius, Pierre Schembri-Wismayer, Lucienne Attard, et al. Negative poisson's ratios in tendons: an unexpected mechanical response. *Acta biomaterialia*, 24:201–208, 2015.

[34] Michelle Vella Wood, Aaron Casha, Alfred Gatt, Cynthia Formosa, Nachiappan Chockalingam, Joseph N Grima, and Ruben Gatt. 3d printed clamps to study the mechanical properties of tendons at low strains. *physica status solidi (b)*, 256(1):1800159, 2019.

[35] DR Veronda and RA Westmann. Mechanical characterization of skin—finite deformations. *Journal of biomechanics*, 3(1):111–124, 1970.

[36] Caroline Lees, Julian FV Vincent, and J Eric Hillerton. Poisson's ratio in skin. *Bio-medical materials and engineering*, 1(1):19–23, 1991.

[37] JL Williams and JL Lewis. Properties and an anisotropic model of cancellous bone from the proximal tibial epiphysis. 1982.

[38] Colin Wiebe and G Wayne Brodland. Tensile properties of embryonic epithelia measured using a novel instrument. *Journal of biomechanics*, 38(10):2087–2094, 2005.

[39] Kate Patten and Tim Wess. Suprafibrillar structures of collagen, evidence for local organization and auxetic behaviour in architectures. *Journal of Biophysical Chemistry*, 2013, 2013.

[40] T Christian Gasser, Ray W Ogden, and Gerhard A Holzapfel. Hyperelastic modelling of arterial layers with distributed collagen fibre orientations. *Journal of the royal society interface*, 3(6):15–35, 2006.

[41] David R Nolan, Artur L Gower, Michel Destrade, Ray W Ogden, and JP McGarry. A robust anisotropic hyperelastic formulation for the modelling of soft tissue. *Journal of the mechanical behavior of biomedical materials*, 39:48–60, 2014.

[42] Marcos Latorre, Xabier Romero, and Francisco J Montans. The relevance of transverse deformation effects in modeling soft biological tissues. *International Journal of Solids and Structures*, 99:57–70, 2016.

[43] K Yu Volokh. On arterial fiber dispersion and auxetic effect. *Journal of biomechanics*, 61:123–130, 2017.

[44] Shengsheng Xiao, Yue Shao, Bo Li, and Xi-Qiao Feng. A micromechanical model of tendon and ligament with crimped fibers. *Journal of the mechanical behavior of biomedical materials*, 112:104086, 2020.

[45] C T Sun and Sijian Li. Three-dimensional effective elastic constants for thick laminates. *Journal of composite materials*, 22(7):629–639, 1988.

[46] Tanaka Mori and Kohichi Tanaka. Average stress in matrix and average elastic energy of materials with misfitting inclusions. *Acta metallurgica*, 21(5):571–574, 1973.

[47] William J Parnell. The eshelby, hill, moment and concentration tensors for ellipsoidal inhomogeneities in the newtonian potential problem and linear elastostatics. *Journal of Elasticity*, 125(2):231–294, 2016.

[48] Toshio Mura. *Micromechanics of defects in solids*. Springer Science & Business Media, 2013.

[49] HM Hsiao and IM Daniel. Elastic properties of composites with fiber waviness. *Composites Part A: Applied Science and Manufacturing*, 27(10):931–941, 1996.

[50] Dajun Zhang, Uday Chippada, and Kenneth Jordan. Effect of the structural water on the mechanical properties of collagen-like microfibrils: a molecular dynamics study. *Annals of biomedical engineering*, 35(7):1216–1230, 2007.

[51] DL Skaggs, M Weidenbaum, James C Iatridis, A Ratcliffe, and Van C Mow. Regional variation in tensile properties and biochemical composition of the human lumbar anulus fibrosus. *Spine*, 19(12):1310–1319, 1994.

[52] Gerhard A Holzapfel, Christian AJ Schulze-Bauer, G Feigl, and Peter Regitnig. Single lamellar mechanics of the human lumbar anulus fibrosus. *Biomechanics and modeling in mechanobiology*, 3(3):125–140, 2005.

[53] Dominique Ambard and Fabien Cherblanc. Mechanical behavior of annulus fibrosus: a microstructural model of fibers reorientation. *Annals of biomedical engineering*, 37(11):2256–2265, 2009.

[54] Pavel Dutov, Olga Antipova, Sameer Varma, Joseph PRO Orgel, and Jay D Schieber. Measurement of elastic modulus of collagen type i single fiber. *PloS one*, 11(1):e0145711, 2016.

[55] Mirit Sharabi, Kelly Wade, and Rami Haj-Ali. The mechanical role of collagen fibers in the intervertebral disc. *Biomechanics of the Spine*, pages 105–123, 2018.

[56] Boris V Shekhonin, Sergey P Domogatsky, Vladimir R Muzykantov, Grigory L Idelson, and Vadim S Rukosuev. Distribution of type i, iii, iv and v collagen in normal and atherosclerotic human arterial wall: immunomorphological characteristics. *Collagen and related research*, 5(4):355–368, 1985.

[57] Daniel H Cortes and Dawn M Elliott. Extra-fibrillar matrix mechanics of annulus fibrosus in tension and compression. *Biomechanics and modeling in mechanobiology*, 11(6):781–790, 2012.

[58] Kazuaki Nagayama, Yujiro Nagano, Masaaki Sato, and Takeo Matsumoto. Effect of actin filament distribution on tensile properties of smooth muscle cells obtained from rat thoracic aortas. *Journal of biomechanics*, 39(2):293–301, 2006.

[59] Paul Ducheyne. *Comprehensive biomaterials*, volume 1. Elsevier, 2015.

[60] Mary K O'Connell, Sushila Murthy, Samson Phan, Chengpei Xu, JoAnn Buchanan, Ryan Spilker, Ronald L Dalman, Christopher K Zarins, Winfried Denk, and Charles A Taylor. The three-dimensional micro-and nanostructure of the aortic medial lamellar unit measured using 3d confocal and electron microscopy imaging. *Matrix Biology*, 27(3):171–181, 2008.

[61] Adrien Baldit. Micromechanics of the intervertebral disk. In *Multiscale Biomechanics*, pages 455–467. Elsevier, 2018.

[62] Robert B Daroff and Michael J Aminoff. *Encyclopedia of the neurological sciences*. Academic press, 2014.

[63] Mirit Sharabi. Structural mechanisms in soft fibrous tissues: A review. *Front. Mater. 8: 793647. doi: 10.3389/fmats*, 2022.

[64] Carl T Herakovich. Composite laminates with negative through-the-thickness poisson's ratios. *Journal of Composite Materials*, 18(5):447–455, 1984.

[65] P Kwon and CKH Dharan. Effective moduli of high volume fraction particulate composites. *Acta metallurgica et materialia*, 43(3):1141–1147, 1995.

[66] JW Ju and K Yanase. Micromechanics and effective elastic moduli of particle-reinforced composites with near-field particle interactions. *Acta Mechanica*, 215(1):135–153, 2010.

[67] Fatemeh Saadat, Victor Birman, Stavros Thomopoulos, and Guy M Genin. Effective elastic properties of a composite containing multiple types of anisotropic ellipsoidal inclusions, with application to the attachment of tendon to bone. *Journal of the Mechanics and Physics of Solids*, 82:367–377, 2015.

[68] Kelsey D Hamilton, Adam J Chrzan, and Arthur J Michalek. Reflected cross-polarized light microscopy as a method for measuring collagen fiber crimp in musculoskeletal tissues. *Journal of the Mechanical Behavior of Biomedical Materials*, 125:104953, 2022.